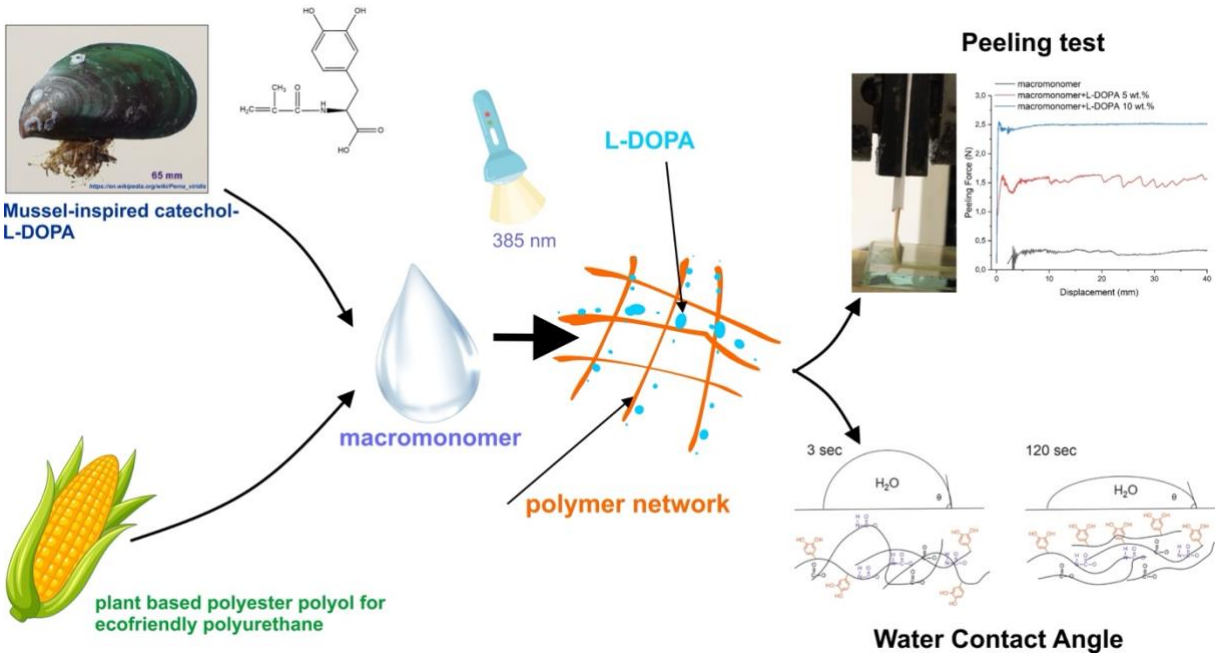

Injectable and photocurable precursors with their improved adhesive elastomeric films by nature-inspired marine mussels chemistry

*Gokhan Demirci, Malwina J. Niedźwiedź, Nina Stefaniak, Peter Sobolewski[$], Miroslawa El Fray**

Department of Polymer and Biomaterials Science, Faculty of Chemical Technology and Engineering, West Pomeranian University of Technology in Szczecin,
Al. Piastów 45, 70-311 Szczecin, POLAND
[$] current address: The Jackson Laboratory,
10 Discovery Dr, Farmington, CT 06032, Connecticut, United States of America
*corresponding author: mirfray@zut.edu.pl

Abstract

Photocurable materials, capable of being delivered as liquids and rapidly cured *in situ* within seconds using UV light, are garnering increased interest in advanced minimally invasive

procedures. Examining living organisms to extract novel principles and technologies, and subsequently applying them into synthetic materials to enhance their performances holds a central position in biomimetics (bioinspiration). In this exploration, we delve into the multifaceted world of marine mussel adhesion, emphasizing the pivotal role of 3,4-dihydroxy-L-phenylalanine (L-DOPA) in adhesive proteins. Simultaneously, we navigated the promising realm of elastomers derived from fatty acid dimers. 90° peeling test and fluorescence microscope indicate that the adhesiveness of the catechol-containing samples (5% and 10%) to the hydrophilic surface *versus* control samples were ~4 and 8 times higher, respectively, as compared to within the tested group. Overall, our results suggest that the incorporation of methacrylated L-DOPA in the synthesis of photocured elastomeric networks leads to lower water contact angle and improved adhesiveness, creating new avenues for potential biomedical applications.

Key words: fatty acid dimers, telechelic macromonomer, marine mussel adhesives, methacrylated L-DOPA, water contact angle, adhesiveness, fluorescence microscopy

Corresponding author: mirfray@zut.edu.pl

1. Introduction

The pursuit of innovative biomimetic materials has spurred a convergence of research efforts, drawing inspiration from the diverse wonders of the natural world [1–3]. These innovative materials has led researchers to use in various scientific disciplines [4–7]. Especially, the biomedical field is witnessing a growing interest in developing adhesives that can effectively bond biological tissues or medical devices in dynamic environments. The remarkable adhesion exhibited by the bio-adhesives has motivated scientists to investigate the potential translation of these natural principles into innovative medical adhesives [8–14].

Among the remarkable contributors to this evolving landscape are marine mussels, particularly admired for their extraordinary adhesion in challenging aquatic environments [15, 16]. This adhesive prowess is primarily attributed to a unique set of proteins, wherein 3,4-dihydroxy-L-phenylalanine (L-DOPA) plays a central role [17]. The inherent biocompatibility

and adhesive strength of L-DOPA make it an attractive candidate for biomedical applications, ranging from surgical adhesives and wound closure materials to drug delivery systems [18, 19]. These properties have inspired materials scientists to investigate how synthetic mimics of these protein glues can be made and applied in a biomedical setting [3, 14, 19–22].

Concurrently, elastomers derived from fatty acid dimers have emerged as an intriguing avenue in biomaterials research [23–26]. Fatty acid dimers, resulting from the dimerization of unsaturated fatty acids, possess a molecular structure that imparts flexibility and strength to resulting elastomers. These elastomeric materials exhibit a balance between flexibility and strength, making them well-suited for medical applications [27–29]. The inherent biocompatibility of fatty acid-based elastomers further enhances their appeal for use in medical applications. By drawing inspiration from the structural intricacies of fatty acid dimers, scientists are delving into the development of elastomers that mimic the resilience and flexibility found in biological tissues [30–33].

We have previously developed injectable and photocurable ester-urethane macromonomers based on fatty acid derivatives obtained from vegetable oils and their photo-crosslinked elastomeric films [34]. However, the adhesiveness of the obtained biomaterials was low due to their chemical nature. Therefore, integrating insights from both marine mussel adhesion and fatty acid dimer-based elastomers, this article endeavors to contribute to the expanding knowledge base in biomimetic materials, fostering innovation in biomedical applications with a particular focus on advanced elastomeric materials with adhesive property.

In this article, synthesis and characterization of elastomeric networks consisting dimerized fatty acid derived macromonomer and the nature-inspired adhesion of marine mussels, is discussed with a specific focus on the L-DOPA as a key component in their adhesive proteins. We also examined the effect of L-DOPA concentration on the injectability of the precursors. Furthermore, we explore the hydrophilicity by water contact angle and adhesive strength by

90° peeling test of the obtained materials as well as L-DOPA localization on the photocured elastomeric material by fluorescence microscopy.

2. Experimental Section

2.1. Materials

Dimer-linoleic-acid-based polyester polyol (Priplast 1838) was kindly provided by Cargill Bioindustrial (The Netherlands). Isophorone diisocyanate (98%) (IPDI), 2-hydroxyethylmethacrylate (97%) (HEMA) and silicagel were purchased from Merck KGaA (Germany). Phenothiazine (PTZ), acryloyl chloride, diethyl ether, triethylamine (TEA), methacryloyl chloride, glacial acetic acid and zinc (II) acetyloacetonate (ZnAc) and 3,4-dihydroxyl-L-phenylalanine (L-DOPA) were purchased from Sigma Aldrich (Poznań, Poland). Photoinitiator Omnirad 2022 was purchased from IGM resins (Netherlands). Borax is purchased from Alfa Aesar (Germany). Ethyl acetate (EtOAc), sodium carbonate, magnesium sulfate and ethanol were purchased from Chempur (Poland). HEMA was used after distillation under reduced pressure; all other reagents were used as received.

2.2. Synthesis of the components

2.2.1. Synthesis of telechelic ester-urethane macromonomer

The synthesis of telechelic ester-urethane macromonomer (PrZnAc) was performed in two steps based on our previous work [34]. Briefly, in the first step, 25 g (0.013 mmol) of polyester polyol (Priplast 1838) was reacted with 6.5 ml (0.052 mmol) of IPDI by ZnAc catalyst (2 mol% calculated relative to amount of polyester polyol). In the second step, 6 mg (0.03 mmol) of phenothiazine (a polymerization inhibitor), a second aliquot of a catalyst (the same mol% as in first step), and 6.6 ml (0.054 mmol) of 2-hydroxyethyl methacrylate (HEMA) were introduced, while protecting the reaction from the light. Progress of the reaction was monitored by tracking the ratio between FT-IR absorbance at 2262 cm^{-1} (A_{2262}), which corresponds to N=C=O

vibration in isocyanate groups of IPDI, and at 1526 cm^{-1} (A_{1526}), which corresponds to N-H bending vibrations of the formed urethane bonds. The macromonomer was then precipitated into four-fold excess of ice-cold methanol three times and any residual solvent was evaporated under reduced pressure at 50 °C.

2.2.2. Synthesis of methacrylated L-DOPA

The synthesis of N-methacryloyl 3,4-dihydroxyl-L-phenylalanine as follows:1.15 g (5.69 mmol) of $Na_2B_4O_7$ was dissolved in 30 ml of water. The solution was degassed with argon for 30 minutes, after which 0.592 g (3.0 mmol) of L-DOPA was added and stirred for 15 minutes. 0.317 g (3.0 mmol) of Na_2CO_3 was then added, the solution was cooled to 0 °C and 0.3 ml (3.0 mmol) of methacryloyl chloride was slowly added with stirring. The pH of the solution was maintained above 9 with Na_2CO_3 during the reaction. After stirring for 1 hour at room temperature, the solution was acidified to pH 2 with concentrated HCl. The mixture was extracted with ethyl acetate three times. After washing with 0.1 M HCl and drying over anhydrous $MgSO_4$, the solvent was removed in vacuo to yield crude light brown solid. The product was further purified by elution from a silica gel column with dichloromethane (DCM) and methanol (95:5 v/v). After evaporating the solvent, a white, sticky solid was obtained with a product yield of 35%. Chemical structure of the obtained methacrylated L-DOPA (Figure 1) was confirmed by FTIR and proton NMR spectroscopy.

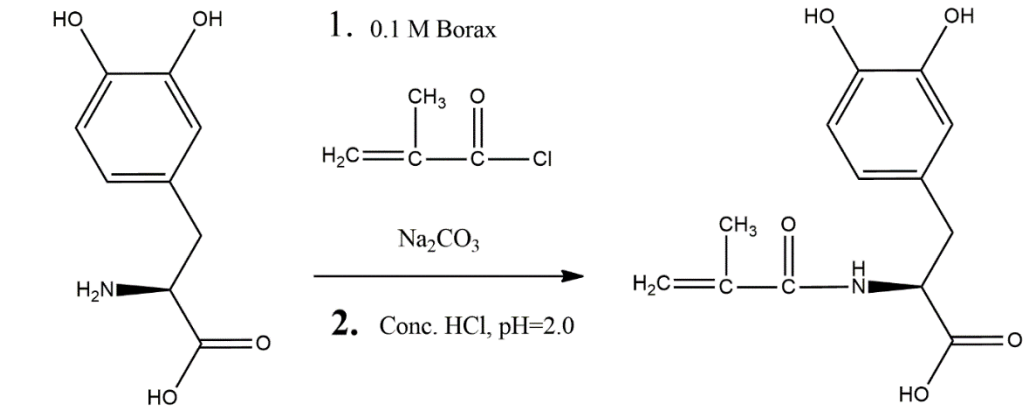

Figure 1 Reaction scheme of methacrylation of L-DOPA.

2.3. Photocuring process

Crosslinked films were prepared according to the following procedure: PrZnAc macromonomer (~20 g) dissolved in EtOAc and various ratios of methacrylated-L-DOPA (5 and 10 wt.%) was mixed homogenously in 25 ml EtOAc. Then, photoinitiator 2% w/w (Omnirad 2022) in EtOAc was inserted into the mixture. Residual solvent was evaporated under reduced pressure after a homogenous mixture was obtained. Then, the films were produced by injecting the final viscous precursor onto glass plate and spreading with a steel applicator (gap thickness: 1 mm). The precursor was then irradiated with a DYMAX Bluewave LED Prime UVA (USA) light source, with a narrow spectral range and maximum intensity at a wavelength λ_{max} of 385 nm. The intensity of the radiation was adjusted to 20 mW/cm^2 and monitored by a radiometer, AktiPrint (Technigraf GmbH, Germany). Photocuring was carried out under air atmosphere. The exposure time was 150 seconds for across the entire plate (10 cm x 20 cm).

2.4. Characterization methods

Fourier transform infrared spectroscopy (FTIR) was performed by using BRUKER ALPHA Platinum apparatus (Germany) at room temperature in the range of 4000–600 cm^{-1}, at a

resolution of 2 cm^{-1} and using 32 scans. Liquid (viscous) macromonomer was analyzed in transmission mode, after injecting material between NaCl plates. Spectra of films after photocuring were obtained using reflection mode and the ATR snap-in with diamond crystal. Spectra were analyzed using EZ OMNIC software.

Proton nuclear magnetic resonance (^{1}H NMR) spectra of the obtained macromonomer and methacrylated L-DOPA were recorded using Bruker DPX HD-400 MHz. The instrument was equipped with a 5 mm Z-gradient broadband decoupling inverse probe. All experiments were conducted at 25 °C. Samples for NMR were prepared by dissolving approx. 50 mg of macromonomer in 0.7 ml of $CDCl_3$-*d* and 20 mg of methacrylated-L-DOPA in 0.7 ml of DMSO-d_6.

Assessing the injectability of a viscous compositions, a standard 10 ml duoNEX (Zarys, Zabrze, Poland) syringe and Sterican® (14 and 18G) needles assembly are employed in a controlled test procedure. The viscous liquid samples maintained undergo an injection process using a specified syringe and needle configuration at 23 °C. The force required to inject the liquid through the needle is measured using a force measurement device which is an Instron 3366 (United Kingdom) with a 500 N load cell, at crosshead speed of 10 mm/min.

The wettability of thin films was evaluated with the use of the KRUSS DSA100 Drop Shape Analyzer. The tests were performed following the BS EN 828:2013 standard: 2 μL droplet of distilled water was spotted on the sample. The camera incline and magnification were set to +1 degree and 7x, respectively. The laboratory temperature was 23.5 °C, and the drop fit method was "tangent 1". The results are averages of ten measurements and the chosen data was written down after 3 s and 120 s.

In the evaluation of adhesive properties of materials on hydrophobic (polystyrene) and hydrophilic (polyvinyl alcohol) (PVA) surfaces, a standardized (ASTM D2861) 90° peel test method was employed. Initially, both substrates are meticulously prepared to ensure cleanliness

from contaminants. The specimens were subjected to a peel test using customized equipment that measures the force required to separate the bonded surfaces.

Fluorescence microscopic observations of catecholamines within the cured films were performed by a modified method. Due to high autofluorescence of the obtained materials, the boronic ester method [35] for confirming catechol presence was not possible. As a result, we developed an alternative method to confirm both the presence of catechol units on the surface of crosslinked films, as well as their functionality and reactivity. We used an amine functionalized far-red dye (ATTO 643-amine, ATTO-TEC GmbH, Siegen Germany) which is hydrophilic, has a high quantum yield, and the primary amine can attack catechols via by Michael addition or forming a Schiff base [36]. Crosslinked strips (approx. 16 mm by 7 mm, 3 per group) were incubated in 1.5 mL of 10 mM TRIS buffer (pH = 9) with 20 µg/mL of ATTO 643-amine (prepared from 4 mg/mL dye stock in DMSO), overnight, at 37 °C. As a control, additional samples were incubated in parallel in the absence of dye. After staining, samples were rinsed three times with PBS and imaged using the Cy5 fluorescence channel (Ex: 620, Em: 700) of Leica DMi8 inverted microscope (Leica HC PL FLUOTAR 10x/0.32 DRY objective and Leica DEC7000 GT 1920x1440 camera). Two or three fields of view were collected per sample. Image analysis was performed using scientific Python ecosystem, including `aicsimageio`[37], `dask` [38], `napari`[39] , `matplotlib`[40], and `numpy` [41]. We quantified the differences between samples by comparing histograms using Wasserstein distance (also known as "earth mover's distance") using the `scipy` Python library [42]. Python code and example notebook is available at: https://github.com/psobolewskiPhD/Fluorescence_L-DOPA_Assay.

3. Results and Discussion

3.1. Chemical structure of the macromonomer and methacrylated L-DOPA by IR spectroscopy

The FT-IR measurement permitted us to confirm the chemical structure of the obtained macromonomer was consistent with the data derived for macromonomer described in our previous work [43]. FT-IR spectra of the macromonomer containing 5 wt.% methacrylated L-DOPA were compared to the starting macromonomer, and they are presented in Figure 2. Briefly, the absorbance bands at 3368 and 1525 cm^{-1} correspond to stretching vibrations of N-H in urethane groups. The band at 1643 cm^{-1} corresponds to stretching vibrations of C=C from the coupling of HEMA, and methacrylate from methacrylated L-DOPA. Meanwhile, the bands 2921 and 2853 cm^{-1} correspond to stretching vibrations of C-H in $-CH_2$ and $-CH_3$. The band at approx. 1732 cm^{-1} is characteristic for stretching of C=O in ester bonds of the macromonomer. The bands at 1302 and 1049 cm^{-1} correspond to RCOOR' in esters, while the bands at 1236 cm^{-1} and 1168 cm^{-1} correspond to -C-O- stretching vibrations and -C-O-C(=O) stretching vibration, respectively. The spectrum exhibit bands associated with the aromatic structure of L-DOPA, such as the aromatic C-H stretching vibrations in the range of 3100-3000 cm^{-1} and aromatic C-H bending vibrations in the region of 900-700 cm^{-1}. Additionally, the methacrylate functional group contributes distinct bands, including C=O stretching vibrations at approximately 1725 cm^{-1}, and aliphatic C-H stretching vibrations between 3000 and 2800 cm^{-1}. The C-O stretching vibrations arising from the hydroxyl group in L-DOPA is manifested by bands in the 1100-1000 cm^{-1} range. Despite the overlapping bands within the similar characteristic bonds between macromonomer and methacrylated L-DOPA, the specific bands that arise from methacrylated L-DOPA are visible in the FTIR spectra.

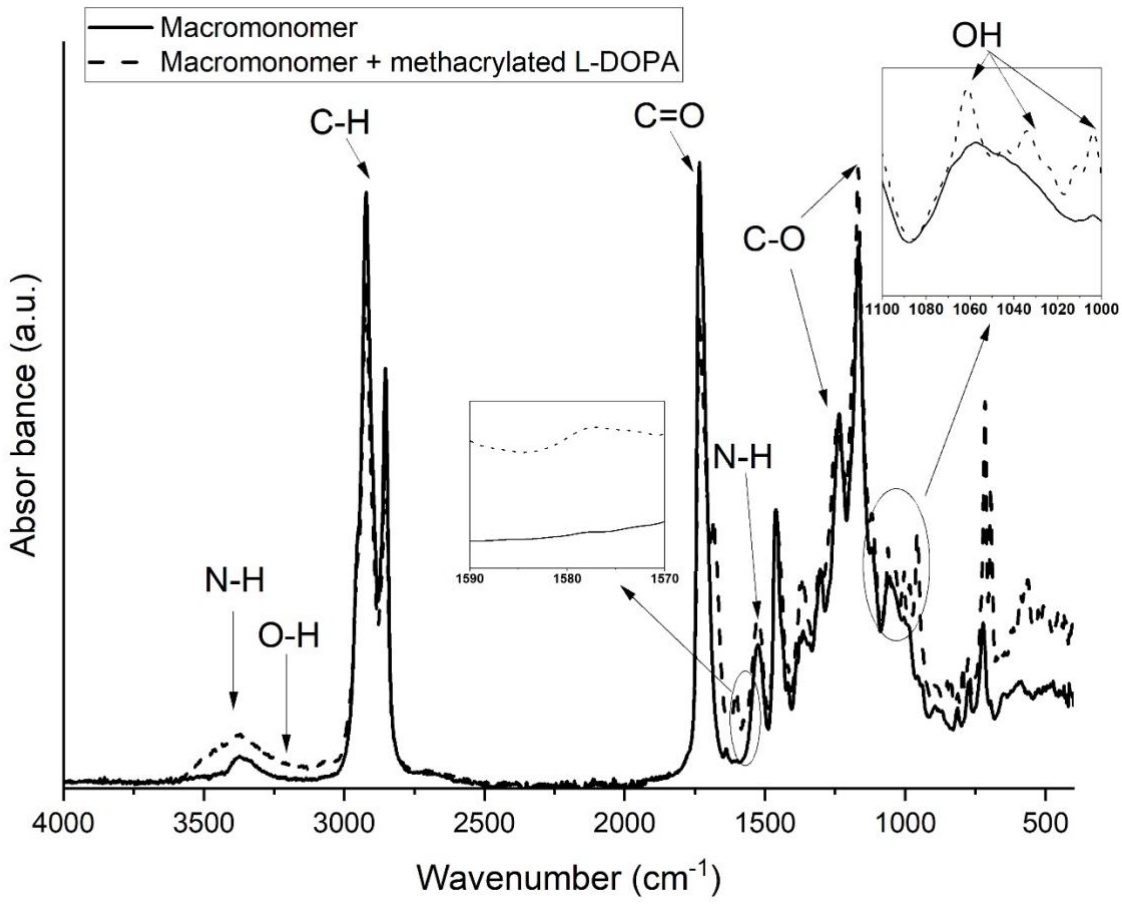

Figure 2 FT-IR spectra of macromonomer and macromonomer with 5 wt.% methacrylayed L-DOPA.

3.2. Chemical structure of the macromonomer and methacrylated-L-DOPA by ^{1}H NMR spectroscopy

The chemical structures of the obtained macromonomer and methacrylated L-DOPA were also confirmed by ^{1}H-NMR spectroscopy. The analysis of NMR spectra also confirmed that the obtained macromonomer had similar structures, consistent with expectations based on our prior work [34]. As a representative example, Figure 3a-b present ^{1}H-NMR spectra of PrZnAc macromonomer and methacrylated L-DOPA. As can be seen from ^{1}H-NMR spectrum, signals at 4.52 and 4.86 ppm confirm the presence of the N-H groups of the urethane bonds, whereas signals at 5.61 and 6.16 ppm confirm the presence of C=C groups from the attachment of

HEMA. Meanwhile, in the ^{13}C-NMR spectrum, the most important signals are found at 129 and 141 ppm, because they correspond to C=C double bonds of the attached HEMA.

In the case of methacrylated L-DOPA (Figure 3b), signal at 7.99 corresponds the N-H groups that has occurred during the methacrylation of L-DOPA. The other characteristic bonds are shown in the spectrum with theirs assignments.

a)

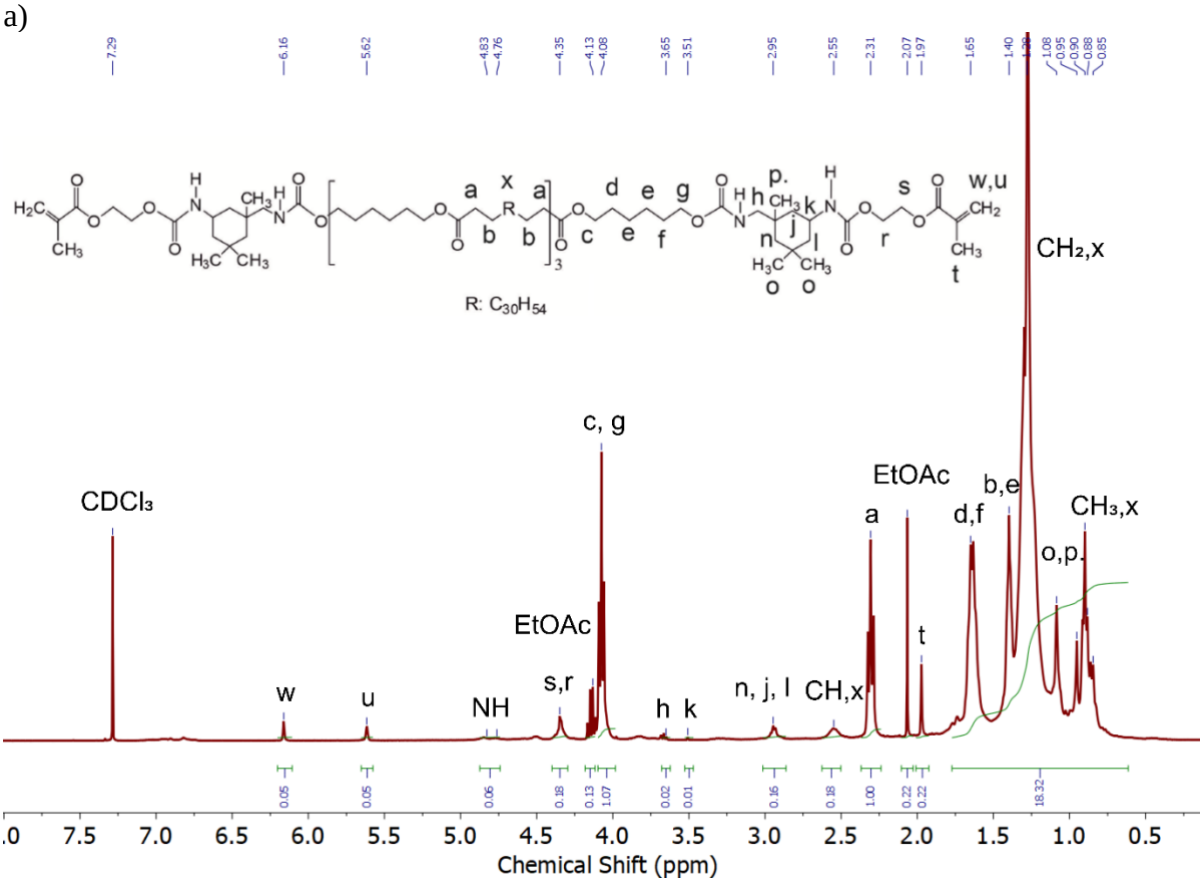

b)

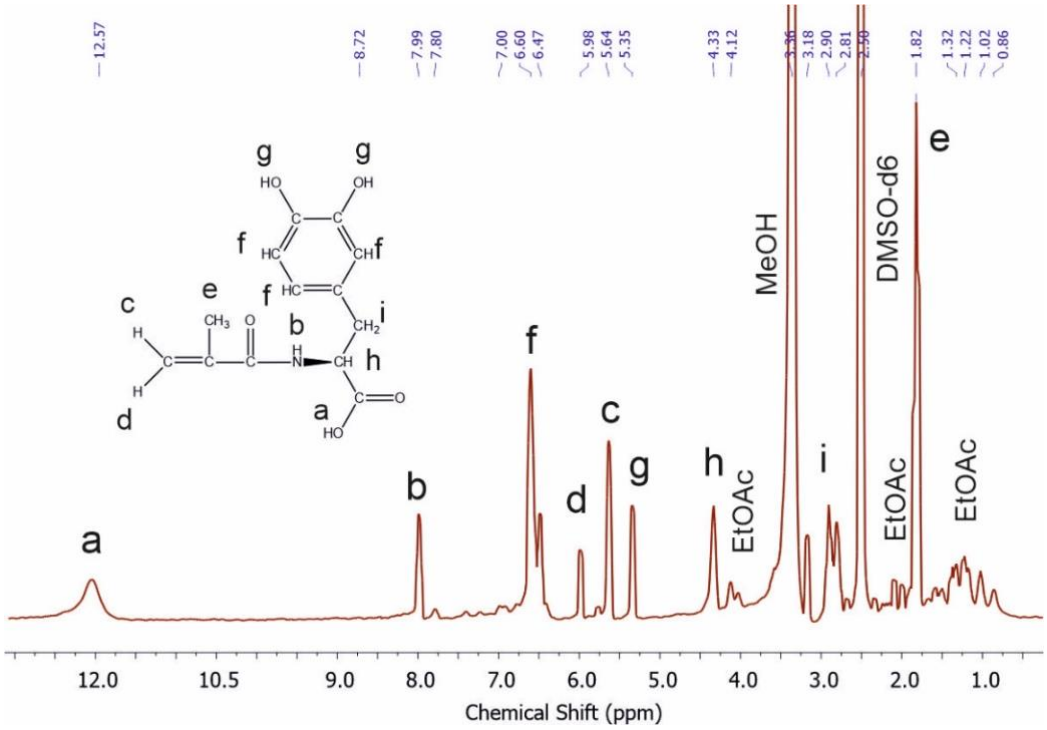

Figure 3 Proton NMR spectra of (a) macromonomer (b) methacrylated L-DOPA with signals assignments.

3.3. Injectability of the compositions

The rheological properties of injectable materials play a pivotal role in medical use, especially for minimally invasive surgeries [44]. These materials must strike a balance, being viscous enough to ensure local retention while remaining sufficiently injectable for proper delivery [45]. Injectability of the macromonomer and macromonomer with methacrylated L-DOPA compositions are determined by measurements of injection force and compression stress, and the results are presented in Figure 4a-c. The injection forces and compression stresses are varied by using different needle sizes: 9G (without needle) (3.5 mm), 14G (2.1 mm) and 18G (1.2 mm). The primary differences between 9G, 14G (gauge) and 18G needles are their size and typical applications. It allows for faster flow rates due to its larger diameter. This makes it suitable for situations requiring rapid fluid administration. The difference in force and compression stress trends between different needles and low L-DOPA levels can be attributed

to the interaction between needle size, material viscosity, and crosslinking density. At low L-DOPA levels, the network is less crosslinked, leading to a softer material that may deform more easily under compression, resulting in lower force and compression stress. Our findings indicate that despite high viscosity of the obtained compositions they exhibit excellent injectability even with up to an 18 G needle where minimally invasive surgical procedures employing relatively large gauges of instruments such as catheters. This suitability may extend future applications of such compositions to various techniques, including laparoscopic and catheter procedures [46–48].

a1

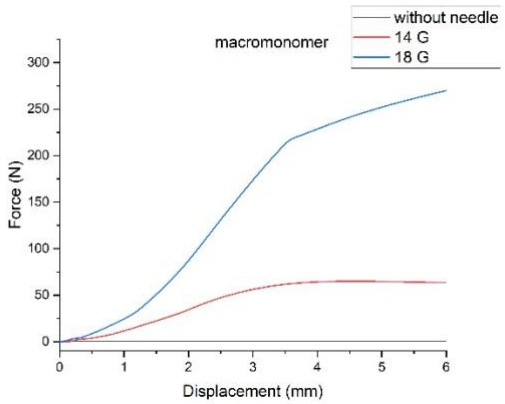

a2

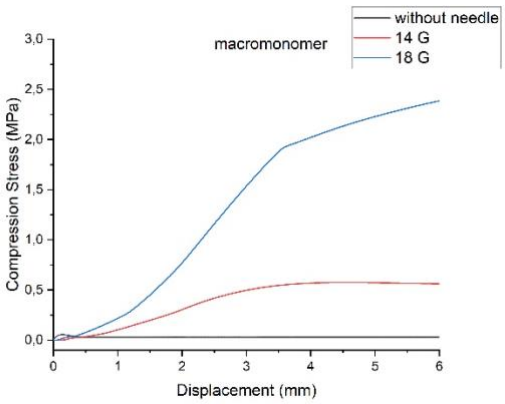

b1

b2

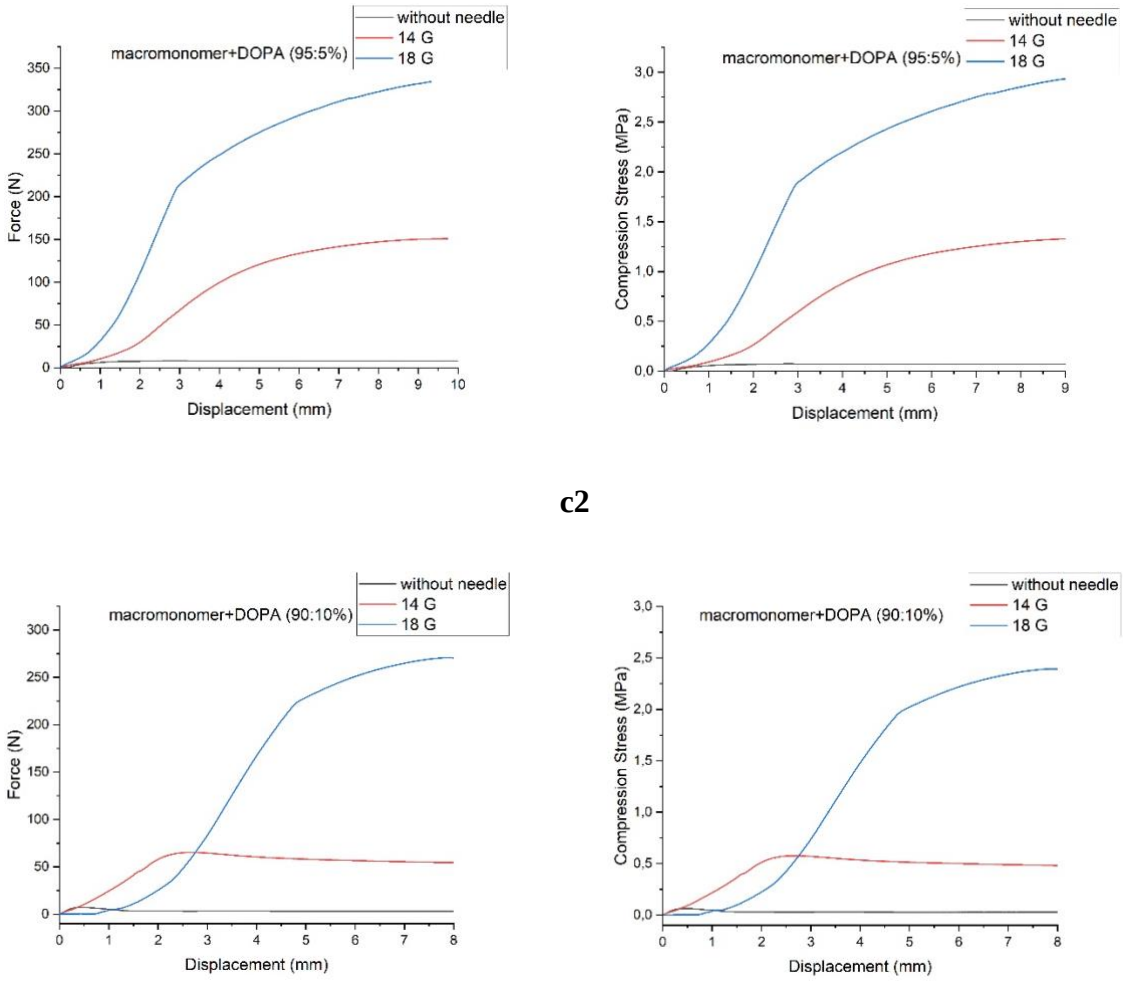

Figure 4 Injection force and compression stress of a1,2) PrZnAc macromonomer, b1,2) PrZnAc macromonomer A+ 5 wt.% methacrylated L-DOPA and c1,2) PrZnAc macromonomer + 10 wt.% methacrylated L-DOPA.

3.4. Chemical structure of photocured elastomeric networks

In order to perform photocuring of the obtained viscous compositions, all of the materials were photocured in air, following the addition of 2% w/w of photoinitiator (Omnirad 2022) (Figure 5).

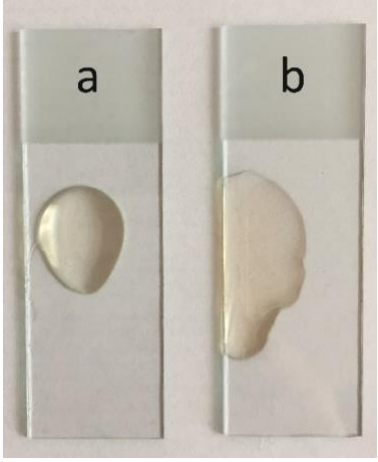

Figure 5 Images of a) macromonomer, b) macromonomer with 5 wt.% methacrylated L-DOPA before photocuring on the glass.

The chemical structures of photocured films were confirmed by ATR FT-IR spectroscopy. Figure 6 shows representative IR spectra of films obtained before/after photocuring of the macromonomer and macromonomer with 5 wt.% methacrylated L-DOPA under air atmosphere. A difference in absorbance of the band at 1643 cm^{-1}, corresponding to stretching vibration of C=C, was observed. The carbon-carbon double bonds present in the macromonomer from the attached HEMA and methacrylate from methacrylated L-DOPA are converted into carbon-carbon bond during photopolymerization process.

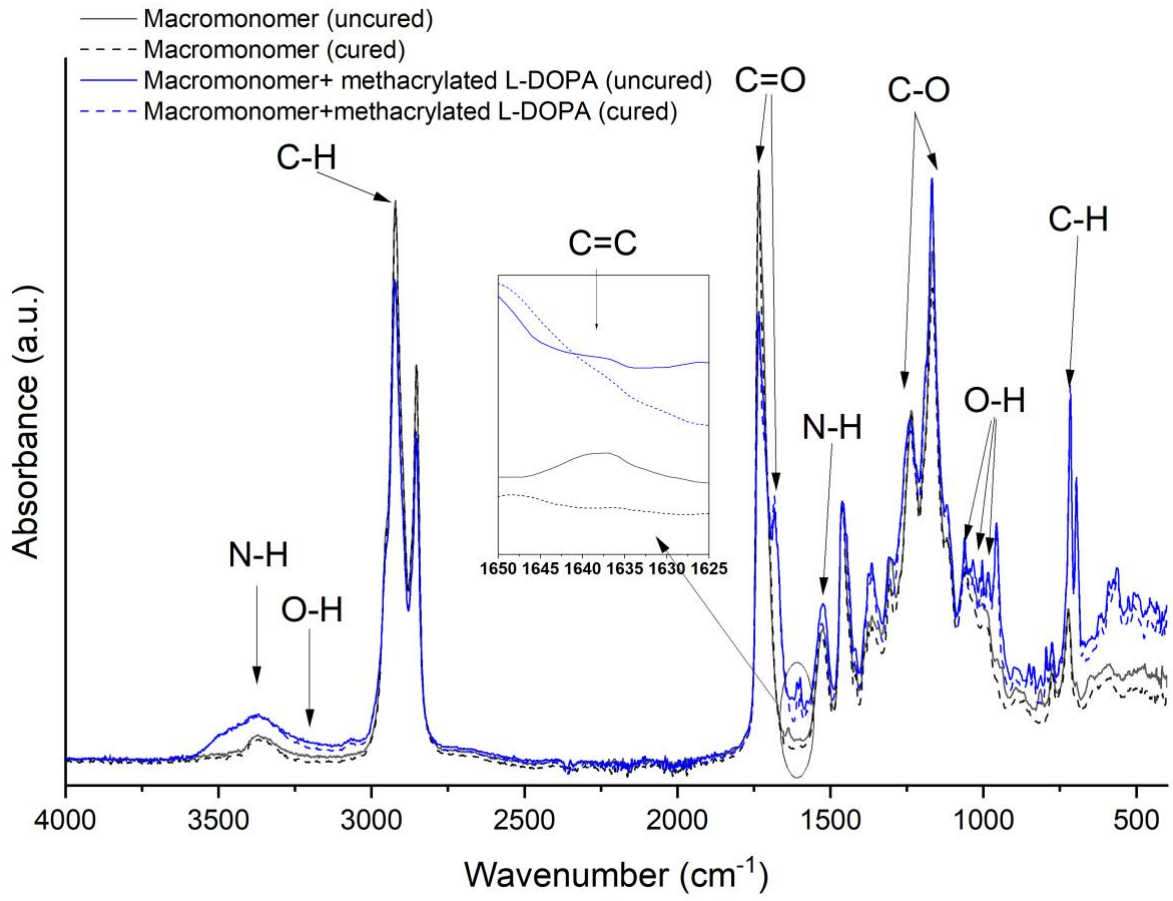

Figure 6 FT-IR spectra of uncured (straight lines) and cured films (dashed lines).

3.5. Assessment of photocured films wettability

Surface wettability is an important parameter determining cell-material interaction in biomedical applications. Low water contact angles, indicating higher wettability, enhance the interaction between the material and biological tissues. This property is particularly advantageous in applications such as tissue scaffolds for regenerative medicine, where close contact between the scaffold and tissue is essential for cell adhesion and proliferation.

The water contact angle data are collected in Table S1 (in Supplementary Information) and show representative water contact angle values for PrZnAc macromonomer and PrZnAc with 5 and 10 wt.% methacrylated L-DOPA. The surface which was in contact with air during photocuring has been assessed. In the case of macromonomer, the side that was in contact with

the air showed hydrophobic nature due the long fatty acid chains. The higher content of L-DOPA increased the hydrophilicity from 108.3±5.4 for macromonomer with 5 wt.% methacrylated L-DOPA to 103.4±7.9 and macromonomer with 10 wt.% methacrylated L-DOPA to 96.6±2.2. The introduction of L-DOPA to macromonomer results in a possible re-organization of the surface within the measured time (**Error! Reference source not found.**). The addition of L-DOPA further decreased, as expected, the surface hydrophilicity of photocured network to 71.8 and 69.2 degree, for the macromonomers that contain with 5 and 10 wt.% L-DOPA, respectively (Table 1). This can be explained by presence of dihydroxy functionality of catechol within L-DOPA (**Error! Reference source not found.**, in Supplementary Information) which enables it to form strong hydrogen bonds with water [49] during the measurement time. Additionally, the aromatic ring participates in cation–π interactions with positively charged ions, a potent non-covalent interaction particularly effective in water. According to the Van Damme et al. different advancing and receding contact angles are often observed when dynamic contact angles of polymers at the air-water interface are measured [50].

3.6. Peeling Test

The adhesion strength is mainly attributed to the strong adhesion and cohesion of the network structures [51]. The peel force values provide a representative measure of adhesive performance on both hydrophobic polystyrene (PS) and hydrophilic polyvinyl alcohol (PVA) surfaces. The test results are presented in Figure . As shown in Figure a, the highest adhesive material on the PS surface is observed with the macromonomer only. This could be due to the hydrophobic nature of the macromonomer, which interacts with the hydrophobic surface through hydrophobic interactions. The addition of a more hydrophilic component (methacrylated L-DOPA) in the composition shows lower interaction with PS, and the peeling force decreases by almost 2.7 times compared to the macromonomer itself.

Regarding the peeling force on PVA (Figure b), the highest peeling force is observed in the sample containing macromonomer with 10 wt.% of methacrylated L-DOPA. Due to the presence of L-DOPA that contains catechol units, the material-surface interaction has increased by approximately 4 and 8 times after the addition of 5 wt.% and 10 wt.%, respectively, compared to the neat macromonomer. The possible physical interactions include hydrogen bonding between the catechol unit and hydroxyl groups of PVA, leading to high adhesion.

It is important to note, that significant increase in adhesiveness of catechol-containing samples (4 to 8 times higher) to hydrophilic surfaces demonstrates potential for strong and durable bonding in moist environments. This is crucial for applications like surgical adhesives, dental restorations, and coatings for medical devices where robust and reliable adhesion is necessary.

a)

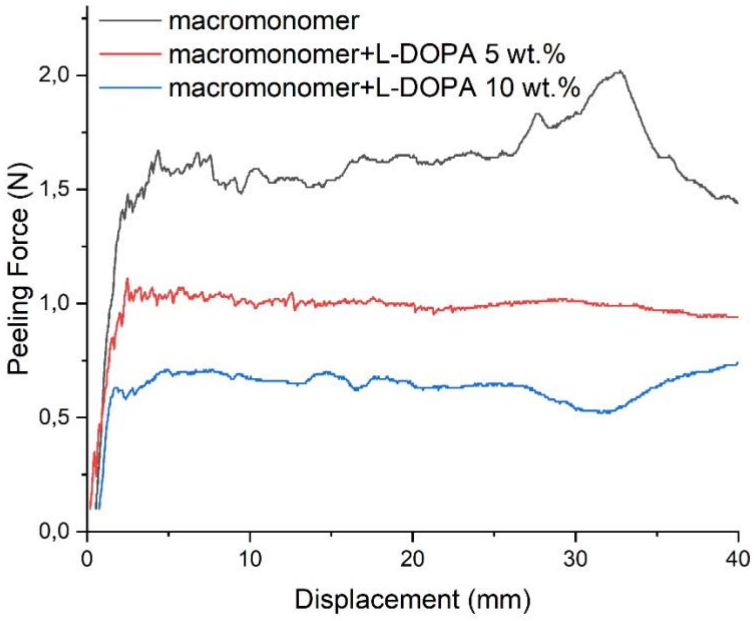

b)

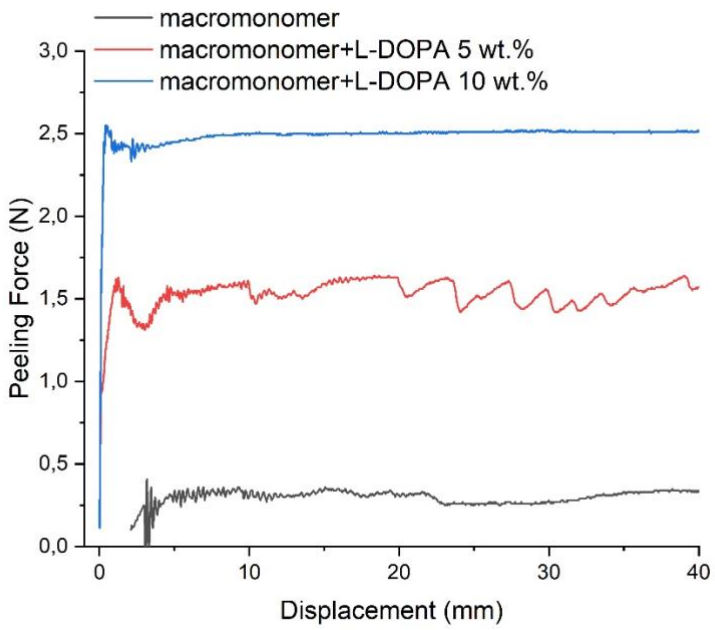

Figure 7 90° peeling test of the photocured films on a) polystyrene (PS) b) polyvinyl alcohol (PVA).

3.7. Fluorescence microscopy

In order to confirm the presence of biofunctional catechol units from L-DOPA on the surface of cured films, we stained samples with an amine-functionalized far-red dye (ATTO 643-amine, imaged in the Cy5 fluorescence channel). If reactive catechols were present on the surface of the cured films, then the primary amine of the dye would be able to attack them via Michael addition or by forming a Schiff base, resulting in an increase in fluorescence (Figure 8)(in Supplementary Information Figure S2). Importantly, this is the same mechanism that is responsible for the pro-adhesive role of catechols [36], so our assay can confirm both the presence and biofunctionality of the L-DOPA units on the surface of cured films. Using the developed assay, we confirmed a marked increase in fluorescence emission in the Cy5 channel for L-DOPA-containing films (median fluorescence 29 and 31 for 5% L-DOPA and 10% L-DOPA), as compared to controls films (median fluorescence 8), indicating the presence of

conjugated amine-functionalized ATTO 643 dye. We further quantified the differences between histograms by Wasserstein distance (also known as "earth mover's distance" or EMD), which can be considered the cost or energy needed to convert one histogram into another [52]. It takes into account both the number of pixels and the intensity difference (distance they need to be moved). Using this approach, we were able to confirm an increase in fluorescence with the higher amounts of L-DOPA: Wasserstein distances for films containing 5% L-DOPA and 10% L-DOPA were 2 and 2.8 times higher versus controls (no L-DOPA), respectively, as compared to within group comparisons and the Wasserstein distance between the two L-DOPA concentrations was 86% of the distance between 5% L-DOPA and the control group, indicating close to a dose response (Figure 8). Finally, the fluorescence of the control samples without L-DOPA units was similar to that of sham stained (no dye) samples, confirming specificity of the fluorescence signal to the bioavailability of L-DOPA catechol groups. Overall, we conclude that this fluorescence assay indicates the presence and biofunctionality of L-DOPA catechol units on the surface, with greater amount of L-DOPA content resulting in higher bioavailability of L-DOPA catechol units on the surface of cured films.

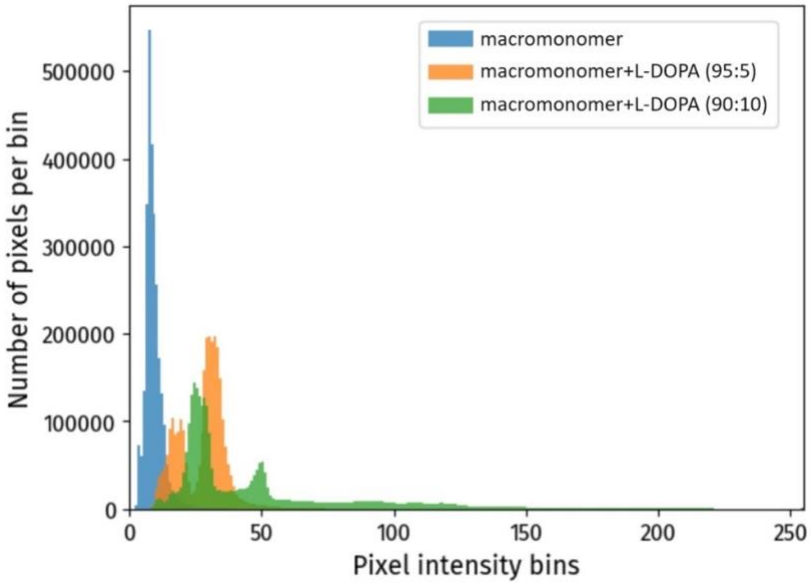

Figure 8 Dynamic clustering of histogram data based on adaptive squared Wasserstein distances.

4. Conclusion

We report here on the synthesis and characterization of the macromonomer containing an ester-urethane linkage and marine mussel-inspired methacrylated L-DOPA units. FTIR and NMR studies indicated that the components were successfully obtained using respective synthesis protocols. Compositions prepared from individual components showed good injectability through 18 G needle. Furthermore, photocuring of the combination of these two components was performed to produce elastomeric films. According to the 90° peeling test and fluorescence microscopy, the elastomeric films obtained from the macromonomer with 5 wt.% and 10 wt.% methacrylated L-DOPA showed better adhesiveness compared to those prepared from the macromonomer alone. All discussed results showed the possibility of such an advance biomimetic materials production and a particular emphasis on their transformative potential usage in medical applications such as wound closure, bone repair, and as a sealant for internal bleeding where the injectability and adhesiveness are desirable features.

CRediT authorship contribution statement

Gokhan Demirci – conceptualization, data curation, methodology, writing – review & editing, **Malwina J. Niedźwiedź** – investigation, analysis, **Nina Stefaniak** – investigation**, Peter Sobolewski,** writing – review & editing, **Miroslawa El Fray** – conceptualization, formal analysis, supervision, writing – review & editing, funding acquisition.

Conflict of Interest

M. El Fray is co-inventor of patents that are licensed to PolTiss Sp. z o.o.

Acknowledgements

This work has been supported by research project OPUS17 from the Polish National Science Center (Narodowe Centrum Nauki) „Hybrid and elastomeric polymer networks: synthesis, structure and properties", UMO-2019/33/B/ST5/01445. The authors thank Krzysztof Gorący for performing peeling test, Prof. Karol Fijałkowski, (Faculty of Biotechnology and Animal Husbandry, ZUT) for access to the multi-functional plate reader.

Data availability

Data will be made available on request.

References

1. Suresh Kumar N, Padma Suvarna R, Chandra Babu Naidu K, et al (2020) A review on biological and biomimetic materials and their applications. Appl Phys A 126:445. https://doi.org/10.1007/s00339-020-03633-z

2. Naik RR, Singamaneni S (2017) Introduction: Bioinspired and Biomimetic Materials. Chem Rev 117:12581–12583. https://doi.org/10.1021/acs.chemrev.7b00552

3. Demirci G, Niedźwiedź MJ, Kantor-Malujdy N, El Fray M (2022) Elastomer–Hydrogel Systems: From Bio-Inspired Interfaces to Medical Applications. Polymers (Basel) 14:1822. https://doi.org/10.3390/polym14091822

4. Liu S, Yu J-M, Gan Y-C, et al (2023) Biomimetic natural biomaterials for tissue engineering and regenerative medicine: new biosynthesis methods, recent advances, and emerging applications. Mil Med Res 10:16. https://doi.org/10.1186/s40779-023-00448-w

5. Das D, Noh I (2018) Overviews of Biomimetic Medical Materials. pp 3–24

6. Sprio S, Sandri M, Iafisco M, et al (2013) Biomimetic materials in regenerative medicine. In: Biomimetic Biomaterials. Elsevier, pp 3–45

7. Rani K (2021) Clinical Approaches of Biomimetic: An Emerging Next Generation Technology. In: Biomimetics. IntechOpen

8. Lu D, Wang H, Li T, et al (2017) Mussel-Inspired Thermoresponsive Polypeptide–Pluronic Copolymers for Versatile Surgical Adhesives and Hemostasis. ACS Appl Mater Interfaces 9:16756–16766. https://doi.org/10.1021/acsami.6b16575

9. Sun A, Hu D, He X, et al (2022) Mussel-inspired hydrogel with injectable self-healing and antibacterial properties promotes wound healing in burn wound infection. NPG Asia Mater 14:86. https://doi.org/10.1038/s41427-022-00434-z

10. Chang K-Y, Chou Y-N, Chen W-Y, et al (2022) Mussel-Inspired Adhesive and Self-Healing Hydrogel as an Injectable Wound Dressing. Polymers (Basel) 14:3346. https://doi.org/10.3390/polym14163346

11. Yang Y, Liang Y, Chen J, et al (2022) Mussel-inspired adhesive antioxidant antibacterial hemostatic composite hydrogel wound dressing via photo-polymerization for infected skin wound healing. Bioact Mater 8:341–354. https://doi.org/10.1016/j.bioactmat.2021.06.014

12. Wang L, Zhao Z, Dong J, et al (2023) Mussel-Inspired Multifunctional Hydrogels with Adhesive, Self-Healing, Antioxidative, and Antibacterial Activity for Wound Healing. ACS Appl Mater Interfaces 15:16515–16525. https://doi.org/10.1021/acsami.3c01065

13. Basak S (2021) Co-evolving with Nature: The Recent Trends on the Mussel-inspired Polymers in Medical Adhesion. Biotechnol Bioprocess Eng 26:10–24. https://doi.org/10.1007/s12257-020-0234-z

14. Pandey N, Soto-Garcia LF, Liao J, et al (2020) Mussel-inspired bioadhesives in healthcare: design parameters, current trends, and future perspectives. Biomater Sci 8:1240–1255. https://doi.org/10.1039/C9BM01848D

15. Li L, Zeng H (2016) Marine mussel adhesion and bio-inspired wet adhesives. Biotribology 5:44–51. https://doi.org/10.1016/j.biotri.2015.09.004

16. Silverman HG, Roberto FF (2007) Understanding Marine Mussel Adhesion. Mar Biotechnol 9:661–681. https://doi.org/10.1007/s10126-007-9053-x

17. Guvendiren M, Brass DA, Messersmith PB, Shull KR (2009) Adhesion of DOPA-Functionalized Model Membranes to Hard and Soft Surfaces. J Adhes 85:631–645. https://doi.org/10.1080/00218460902997000

18. van Vliet EF, Knol MJ, Schiffelers RM, et al (2023) Levodopa-loaded nanoparticles for the treatment of Parkinson's disease. J Control Release 360:212–224.

https://doi.org/10.1016/j.jconrel.2023.06.026

19. Rahimnejad M, Zhong W (2017) Mussel-inspired hydrogel tissue adhesives for wound closure. RSC Adv 7:47380–47396. https://doi.org/10.1039/C7RA06743G

20. Han L, Lu X, Liu K, et al (2017) Mussel-Inspired Adhesive and Tough Hydrogel Based on Nanoclay Confined Dopamine Polymerization. ACS Nano 11:2561–2574. https://doi.org/10.1021/acsnano.6b05318

21. Kaushik N, Kaushik N, Pardeshi S, et al (2015) Biomedical and Clinical Importance of Mussel-Inspired Polymers and Materials. Mar Drugs 13:6792–6817. https://doi.org/10.3390/md13116792

22. Brubaker CE, Kissler H, Wang L-J, et al (2010) Biological performance of mussel-inspired adhesive in extrahepatic islet transplantation. Biomaterials 31:420–427. https://doi.org/10.1016/j.biomaterials.2009.09.062

23. Paraskar PM, Major I, Ladole MR, et al (2023) Dimer fatty acid – A renewable building block for high-performance polymeric materials. Ind Crops Prod 200:116817. https://doi.org/10.1016/j.indcrop.2023.116817

24. Maisonneuve L, Lebarbé T, Grau E, Cramail H (2013) Structure–properties relationship of fatty acid-based thermoplastics as synthetic polymer mimics. Polym Chem 4:5472. https://doi.org/10.1039/c3py00791j

25. Mitsak AG, Dunn AM, Hollister SJ (2012) Mechanical characterization and non-linear elastic modeling of poly(glycerol sebacate) for soft tissue engineering. J Mech Behav Biomed Mater 11:3–15. https://doi.org/10.1016/j.jmbbm.2011.11.003

26. Tang S, Li J, Wang R, et al (2022) Current trends in bio-based elastomer materials. SusMat 2:2–33. https://doi.org/10.1002/sus2.45

27. Sokołowska M, Nowak-Grzebyta J, Stachowska E, et al (2023) Enzymatically catalyzed furan-based copolyesters containing dilinoleic diol as a building block. RSC Adv 13:22234–22249. https://doi.org/10.1039/D3RA03885H

28. Meng J, Yao C (2010) Synthesis and properties of hyperbranched polyurethane elastomers based on dimer fatty acid-ethylene glycol polyester diol. e-Polymers 10:. https://doi.org/10.1515/epoly.2010.10.1.349

29. Wang S, Vajjala Kesava S, Gomez ED, Robertson ML (2013) Sustainable Thermoplastic Elastomers Derived from Fatty Acids. Macromolecules 46:7202–7212. https://doi.org/10.1021/ma4011846

30. Prowans P, El Fray M, Slonecki J (2002) Biocompatibility studies of new multiblock poly(ester–ester)s composed of poly(butylene terephthalate) and dimerized fatty acid. Biomaterials 23:2973–2978. https://doi.org/10.1016/S0142-9612(02)00026-1

31. Aleemardani M, Trikić MZ, Green NH, Claeyssens F (2022) Elastomeric, bioadhesive and pH-responsive amphiphilic copolymers based on direct crosslinking of poly(glycerol sebacate)- co -polyethylene glycol. Biomater Sci 10:7015–7031. https://doi.org/10.1039/D2BM01335E

32. Uscátegui Maldonado YL, Díaz Barrera LE, Valero Valdivieso MF, Coy-Barrera E (2023) Synthesis and characterization of polyurethane films based on castor oil-derived polyols with heparin and low-molecular-weight chitosan for cardiovascular implants. J Mater Res 38:3349–3361. https://doi.org/10.1557/s43578-023-01060-3

33. Uscátegui YL, Díaz LE, Valero MF (2019) In vitro and in vivo biocompatibility of polyurethanes synthesized with castor oil polyols for biomedical devices. J Mater Res 34:519–531. https://doi.org/10.1557/jmr.2018.448

34. Niedźwiedź MJ, Demirci G, Kantor-Malujdy N, et al (2022) Fatty-acid-derived ester-urethane macromonomers synthesized using bismuth and zinc catalysts. Eur Polym J 170:111168. https://doi.org/10.1016/j.eurpolymj.2022.111168

35. Córdoba A, Monjo M, Hierro-Oliva M, et al (2015) Bioinspired Quercitrin Nanocoatings: A Fluorescence-Based Method for Their Surface Quantification, and Their Effect on Stem Cell Adhesion and Differentiation to the Osteoblastic Lineage. ACS Appl Mater Interfaces 7:16857–16864. https://doi.org/10.1021/acsami.5b05044

36. Ryu JH, Messersmith PB, Lee H (2018) Polydopamine Surface Chemistry: A Decade of Discovery. ACS Appl Mater Interfaces 10:7523–7540. https://doi.org/10.1021/acsami.7b19865

37. Eva Maxfield Brown, Dan Toloudis, Jamie Sherman, Madison Swain-Bowden TL (2021) AICSImageIO: Image Reading, Metadata Conversion, and Image Writing for Microscopy Images in Pure Python. https://github.com/AllenCellModeling/aicsimageio

38. Team DD (2016) Dask: library for dynamic task scheduling. https://dask.org

39. Napari contributors napari: a multi-dimensional image viewer for python. https://zenodo.org/records/8115575

40. Hunter JD (2007) Matplotlib: A 2D Graphics Environment. Comput Sci Eng 9:90–95. https://doi.org/10.1109/MCSE.2007.55

41. Harris CR, Millman KJ, van der Walt SJ, et al (2020) Array programming with NumPy. Nature 585:357–362. https://doi.org/10.1038/s41586-020-2649-2

42. Virtanen P, Gommers R, Oliphant TE, et al (2020) SciPy 1.0: fundamental algorithms for scientific computing in Python. Nat Methods 17:261–272. https://doi.org/10.1038/s41592-019-0686-2

43. El Fray M, Skrobot J, Bolikal D, Kohn J (2012) Synthesis and characterization of telechelic macromers containing fatty acid derivatives. React Funct Polym 72:781–790. https://doi.org/10.1016/j.reactfunctpolym.2012.07.010

44. McLemore R (2011) Rheological properties of injectable biomaterials. In: Injectable Biomaterials. Elsevier, pp 46–60

45. Raucci MG, D'Amora U, Ronca A, Ambrosio L (2020) Injectable Functional Biomaterials for Minimally Invasive Surgery. Adv Healthc Mater 9:2000349. https://doi.org/10.1002/adhm.202000349

46. Hinderer S, Brauchle E, Schenke-Layland K (2015) Generation and Assessment of Functional Biomaterial Scaffolds for Applications in Cardiovascular Tissue Engineering and Regenerative Medicine. Adv Healthc Mater 4:2326–2341. https://doi.org/10.1002/adhm.201400762

47. Van Damme L, Blondeel P, Van Vlierberghe S (2021) Injectable biomaterials as minimal invasive strategy towards soft tissue regeneration—an overview. J Phys Mater 4:022001. https://doi.org/10.1088/2515-7639/abd4f3

48. Zhou H, Liang C, Wei Z, et al (2019) Injectable biomaterials for translational medicine. Mater Today 28:81–97. https://doi.org/10.1016/j.mattod.2019.04.020

49. Kord Forooshani P, Lee BP (2017) Recent approaches in designing bioadhesive materials inspired by mussel adhesive protein. J Polym Sci Part A Polym Chem 55:9–33. https://doi.org/10.1002/pola.28368

50. Van Damme H., Hogt A., Feijen J (1986) Surface mobility and structural transitions of poly(n-alkyl methacrylates) probed by dynamic contact angle measurements. J Colloid Interface Sci 114:167–172. https://doi.org/10.1016/0021-9797(86)90248-1

51. Xue B, Gu J, Li L, et al (2021) Hydrogel tapes for fault-tolerant strong wet adhesion. Nat Commun 12:7156. https://doi.org/10.1038/s41467-021-27529-5